# Spectroscopy of $Pr^{3+}$-doped Low Phonon Energy Glasses Based on Halides and Sulphides

D.W. Hewak, J.A. Medeiros Neto, B. Samson, J. Wang, H.J. Tate, A. Pearson, W.S. Brocklesby, G. Wylangowski and D.N. Payne

Optoelectronics Research Centre, University of Southampton
Southampton, SO9 5NH United Kingdom

A. Jha, M. Naftaly and S. Jordery
Department of Materials Technology, Brunel University
Uxbridge, Middlesex, UB8 3DH United Kingdom

M. Poulain
Centre d'Etudes des Materiaux Photoniques, University of Rennes
Campus de Beaulieu, 35042 Rennes Cedex France

## ABSTRACT

The optical properties of praseodymium-doped glasses have attracted considerable attention recently for their potential application as a 1.3 micron optical amplifier. As a result, novel glass compositions are being developed and known glass forming systems are being revisited in the quest for a low-phonon-energy glass which may lead to an efficient amplifier. We report here on our spectroscopic evaluation of a series of low-phonon-energy glasses based on halides and sulphides. These results, though driven by the desire for a practical amplifier, provide insight into the application of these glasses not only for telecommunications applications, but also an understanding of the overall optical properties of a low-phonon-energy glass. Using Raman spectroscopy, the vibrational characteristics of the glass host are determined. These results are confirmed through infrared measurements and with phonon sideband measurements. In this way, the non-radiative properties of the rare earth doped glass can be predicted. Absorption measurements across the visible and infrared allow evaluation of the intrinsic loss of these glasses when in fibre form, as well as providing an indication of glass purity. Fluorescence of $Pr^{3+}$-doped glasses, through excitation of the $^3P_0$, $^1D_2$ and $^1G_4$ levels, is measured along with the fluorescence lifetimes. These radiative properties are compared to those predicted by a Judd-Ofelt analysis, which has been performed on all glasses. In this way, this work provides an overall spectroscopic evaluation of the optical properties of low-phonon-energy glasses, leading the way towards a practical device.

## 2. INTRODUCTION

Driven by the quest for a practical and efficient 1.3 micron amplifier, praseodymium-doped low-phonon energy glasses have recently attracted considerable attention[1-9]. Initial interest in fluoride glass optical fibres doped with praseodymium, the PDFA, was generated in 1991 with the announcement of a 1.3 micron amplifier operating with a gain of over 10 dB[1-3] . This host was extremely inefficient however, with a gain coefficient of less than 0.1 dB/mW, compared to the 11 dB/mW achieved with an erbium-doped amplifier operating at 1.55 microns[10]. This work however led to a concerted effort to improve the efficiency through a series of modified ZBLAN and more recently $InF_3$-based glasses, now realized in fibre form[4]. In addition, other glasses, whose decreased non-radiative rates are expected to favour 1.3 micron amplification through a long fluorescence-lifetime are being explored[5-9]. Among these, sulphide glasses based on $Ga_2S_3$ attracted attention as a promising alternate host for the rare-earth praseodymium. For this high index glass, radiative rates are also increased leading to the highest expected quantum efficiencies[6,9].

In our labs and in collaboration with partners in the European Community, we have fabricated and spectroscopically evaluated a wide series of low phonon energy glasses based halides and chalcogenides. Over two hundred bulk samples, of varying composition and $Pr^{3+}$ concentrations have been achieved. Fluoride glasses based on zirconium and hafnium[11], gallium and indium[12]; chloride and mixed halide glasses based on cadmium[13-14]; and sulfide glasses formed from gallium, aluminium or germanium[15-16] were included in this analysis. Understanding of the radiative and non-radiative properties of these glasses for applications at 1.3 microns, leads naturally to an overall understanding of the properties of a low-phonon-energy host, for applications in the second telecommunications window, and also across the visible and infrared spectrum.

## 3. LOW-PHONON-ENERGY GLASSES

In many cases, the search for a low-phonon-energy glass begins through some qualitative knowledge of the physical and optical properties of the potential host. Good transmission in the infrared, a low glass transition temperature and high atomic weights among the glass formers all suggest the possibility of a low-phonon-energy. Principal considerations for a practical device are phonon-energies less than that of ZBLAN (580 $cm^{-1}$), transparency in the visible and NIR, and thermal properties which give fibre drawing a reasonable chance of success. Early work on optical materials for infrared transmission, applied to long-haul telecommunications and short-distance laser power distribution has provided a wealth of possibilities, some of which have already been realized in fiber form[17-19].

**Table 1. Principal Glass Compositions Evaluated in this Work.**

| Glass | Refractive Index | Density ($g/cm^3$) |
|---|---|---|
| $ZrF_3$ | 1.50 | 4.1 |
| $HfF_3$ | 1.51 | 4.5 |
| $GaF_3$ | 1.61 | 6.0 |
| $InF_3$ | 1.49 | 5.0 |
| $CdF_2/Cl_2$ | 1.59 | 4.6 |
| $Ga_2S_3$ | 2.38 | 4.0 |

Through a variety of such sources, a number of promising candidates have been identified and melted. The majority of glasses are based on a series of halide glasses. Bulk samples were fabricated by standard methods in an atmosphere-controlled glove box[20]. Samples of approximately 5 mm thickness were prepared, doped with less than 1000 ppm $Pr^{3+}$ by weight for lifetime measurements and heavily doped for the absorption measurements used in the Judd-Ofelt analysis. Where possible, samples were optically polished on both sides for spectroscopic analysis. Bulk-glass samples from among the chalcogenides were prepared by melting the starting materials in an evacuated and sealed ampoule in an electric furnace and rapidly quenching[21]. For the principal glasses of this study, basic properties are presented in Table 1. Additional glasses studied in the course of this work include mixed halides based on $GaF_3$ and $HfF_4$, pure chloride glasses based on cadmium, sulphide glasses based on $Al_2S_3$ and $GeS_2$ and chalcohalides. Throughout this review, we identify our glass samples by the main component of the glass which represents 30 to 100 mol% of the composition. Dopant concentrations are given in ppm, defined by the total relative weight of the rare earth compound in the sample.

## 4. NON-RADIATIVE PROPERTIES

### 4.1 Initial Evaluation

Our evaluation of glasses as a potential low-phonon-energy host for praseodymium begins with the application of the Szigeti relation which provides an indication of the maximum-phonon-energy by approximating the vibrational frequency of the fundamental modes of a glass structure by a linear diatomic molecule consisting of two point masses[22]

$$\nu_o = (1/2\pi)\,(f/\mu)^{1/2} \qquad (1)$$

Here f is the restoring force between the cations and anions for the glass former (e.g. Cd and F) and $\mu$ is their reduced mass, given by $m_1m_2/(m_1 + m_2)$. Although only approximating the complex glass structure which makes up a multicomponent low-phonon-energy glass, this simple relationship provides an indication of the trend to lower phonon energies for a material formed from high-atomic-weight ions that are weakly bound.

When working within a family of glasses, for example, the halides, the trend towards lower phonon-energies is indicated by combining the clues provided by the Szigeti relation, $T_g$ and the position of the infrared edge. Table 2 provides this data for our series of halide glasses and compares the maximum phonon energy measured by Raman spectroscopy, as described in the next section, to these basic properties.

Some exceptions to the general trends are observed. Substitution of hafnium (atomic weight = 178) for the

lighter zirconium (atomic weight = 91.2) results in little change in phonon energy. On the basis of the difference in reduced mass differences, a shift in maximum phonon energy of 25 $cm^{-1}$ is expected, however no such shift is observed. In this case the mass of the lighter fluorine anion is so much less than either the zirconium or hafnium that substitution of either has little influence on the relative motion. Essentially, the dominant mode of vibration is fixed by the vibrations of fluorine atoms around a fixed cation[23]. This is a general trend for glasses containing a heavy and light ion combination and frequently limits the degree to which the maximum phonon energy of a glass can be reduced without substituting the lighter ion for one with a higher atomic weight. Mixed halide glasses such as those based on $CdF_2$ and $CdCl_2$ provide such a substitution.

**Table 2. Maximum phonon energies and their relationship to the optical and physical properties of a series of halide glasses.**

| Glass Former | Reduced Mass | IR Cut-off ($\mu$m) | Glass Transition (°C) | Maximum Phonon Energy ($cm^{-1}$) |
|---|---|---|---|---|
| $ZrF_4$ | 15.7 | 5.5 | 260 | 580 |
| $HfF_4$ | 17.2 | 7.0 | 330 | 580 |
| $GaF_3$ | 14.9 | 7.8 | 250 | 525 |
| $InF_3$ | 16.3 | 8.2 | 300 | 510 |
| $CdF_2/CdCl_2$ | 16.3 | 9.5 | 130 | 370 |

### 4.2 Raman Spectroscopy

Raman spectra were taken on a commercial triple grating micro-Raman spectrometer. Excitation was typically at a wavelength of 514.5 from an Ar ion laser. The pump laser and the backscattered Raman signal were guided to and from the sample through an adapted microscope, the microscope objective providing a spatial resolution of a few microns[24]. This allowed measurement on small, unpolished samples or directly onto the fibre core.

Figure 1(a) shows the Raman scattered signal from an indium fluoride based glass. In this multicomponent glass, only the vibration at 510 $cm^{-1}$ corresponding to the glass former is resolved, as the structure associated with the stretching and bending modes of the glass modifiers overlap and are obscured. We note a half width of approximately 80 $cm^{-1}$ for this peak, which is typical for the fluoride glasses. Shown in figure 1(b) is the phonon energy for a mixed halide where contributions from both the halide glass formers, cadmium fluoride and cadmium chloride are observed. In contrast, figure 2 shows the vibrational spectrum of a $Ga_2S_3$:$La_2S_3$ based glass. Again the peak associated with the maximum phonon energy clearly dominates, being broad with a full width at half maximum of over 150 $cm^{-1}$. Previous studies[25] of this glass define the maximum phonon energy of the glass at 350 $cm^{-1}$. This can lead to a lower calculated non-radiative rate than is observed experimentally[9]. Our recent measurements on crystallized samples, shown in figure 2 reveal an internal structure to this broad peak and reveal a possible maximum phonon energy of 425 $cm^{-1}$. Similar observations are made for $Al_2S_3$ and $GeS_2$ based glasses, with maximum phonon energies of 500 $cm^{-1}$ and 445 $cm^{-1}$, respectively. Maximum phonon energies of the remaining glasses in this study are given in table 2.

In addition, Raman spectroscopy provides, to some degree, a method of impurity analysis. Figure 3 reveals fluorescence due to impurity rare-earth ions[26]. Figure 2 reveals the fundamental vibration of $SO_2$ at 526 $cm^{-1}$, a common oxide impurity in a sulphide glass[27].

### 4.3 Non-Radiative Decay Rates

A detailed analysis of Raman data can provide considerable insight into the structure and properties of a glass, however it has been said that Raman spectra are easy to make but difficult to interpret[17]. For the purpose of an evaluation of non-radiative decay rates, it is often sufficient and relatively simple to identify the vibration and its

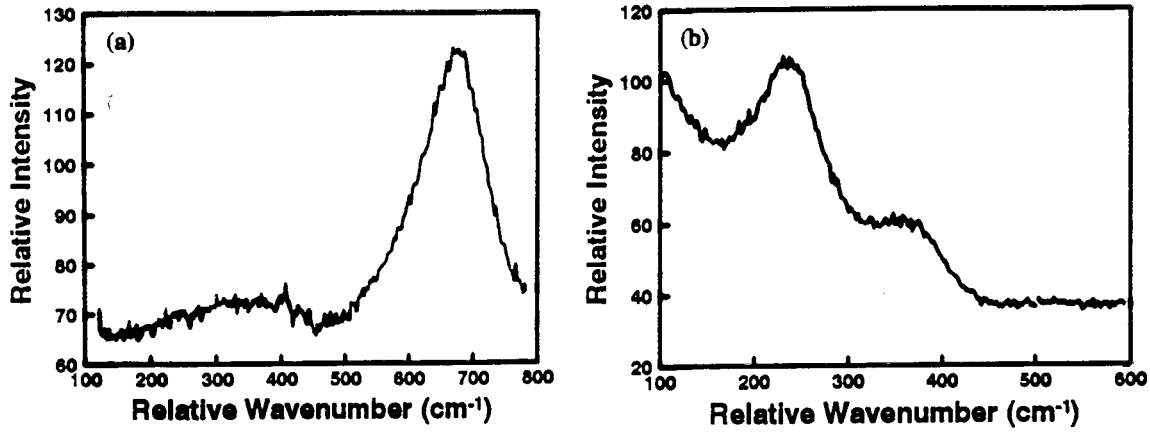


**Figure 1. Vibrational spectrum as measured by Raman spectroscopy for (a) $InF_3$ and (b) $CdF_2/Cl_2$ based bulk glasses.**

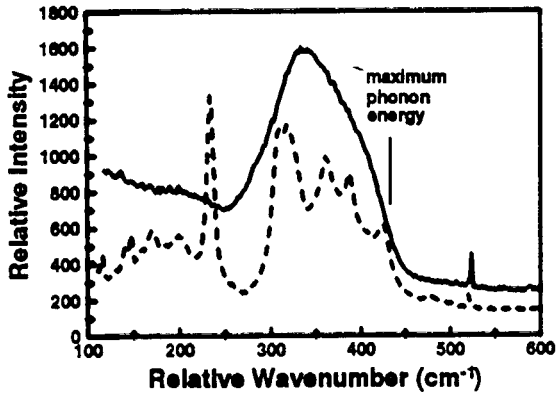


**Figure 2. Vibrational spectrum of undoped $Ga_2S_3$ glass fiber (solid line) and crystallized fiber core (dashed line).**

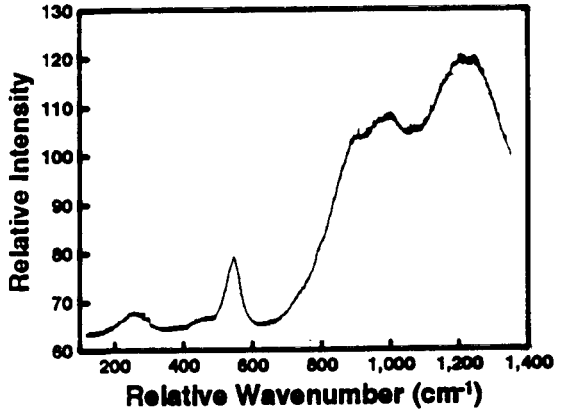


**Figure 3. Impurity identification by Raman spectroscopy showing fluorescence due to rare earth impurities.**

energy which corresponds to the glass former. A rule of thumb which can quickly reveal the propensity of a host to multiphonon decay follows from the number of phonons required to bridge the energy gap to the next lowest level[28]

$$p = \Delta E/h\nu \quad (2)$$

where hν is the maximum phonon energy and ΔE is the energy gap to the next lower energy level. The highest energy and/or most strongly-coupled phonon are expected to make the dominant contribution to multiphonon relaxation. For example with fluoride glasses, $p < 4$, multiphonon decay completely dominates, with relaxation times less than a microsecond. For p = 5-6, multiphonon emission still dominates, but non-radiative lifetimes of 10's to 100's of microseconds are observed. For $p > 7$, millisecond lifetimes are achieved and radiative decay mechanisms begin to contribute or may dominate.

The multiphonon emission in the f-f transitions of rare-earth ions in solids has been described by a number of theoretical treatments[29]. For practical applications, the phenomenological theory applied by Reisfeld[25] is convenient to implement from experimentally measured maximum phonon energies. For a given host at a room temperature, multiphonon decay rates have an exponential dependence

$$W_{mp} = B^{*} \exp[(-\Delta E + 2h\nu)\alpha] \quad (3)$$

where α and $B^{*}$ are experimentally determined parameters which are constant for a given host and independent of

the particular rare earth ion. Here $\alpha$, related to the electron-phonon coupling constant, is relatively constant among all hosts. For $ZrF_4$- and $Ga_2S_3$-based glasses, it is 5.2 x $10^{-3}$ cm and 2.9 x $10^{-3}$ cm, respectively, indicating a lower electron-phonon coupling constant in the sulphide based glass. In contrast, $B^*$ can vary over several orders of magnitude, although within a family of glasses, for example the oxide glasses, it remains within an order of magnitude. For $ZrF_4$- and $Ga_2S_3$-based glasses, $\log_{10}B^* = 8.0$ and 5.1 respectively[25].

In figure 4 we plot non-radiative decay rates of the $^1G_4$ level for the various glasses in this study. For $ZrF_4$ and $Ga_2S_3$ glasses, the $\alpha$ and $B^*$ parameters given above are used. For the remaining fluoride and sulphide glasses, we make the assumption that $\alpha$ and $B^*$ are approximately constant within their respective glass family. It is clear that the mixed halide and sulphide glasses emerge with the lowest non-radiative rates and thus are the leading candidates for efficient lasing and amplification. For these glasses approximately 7 phonons are required to bridge the $^1G_4$ - $^3F_4$ energy gap.

### 4.4 Phonon Sideband Measurements

According to the theory of multiphonon decay, the larger the electron-phonon coupling constant, the larger the rate of non-radiative decay. By phonon sideband measurements, $\Delta E$ and $g$ can be measured directly. In addition, this technique reveals information directly relevant to the ion within its site in the glass structure. Sidebands arise as the result of phonon-assisted absorption and appear as small additional peaks on the shorter wavelength side of the main emission peak. The wavelength difference between the main peak and side-band corresponds to the energy of the phonons directly interacting with the ion. The relative areas of these two peaks yields the coupling constant. Unlike Raman spectroscopy, side-band measurements are difficult to implement and are facilitated by doping with $Eu^{3+}$, with its simpler Stark structure[30], rather than $Pr^{3+}$.

We have prepared a series of $Eu^{3+}$-doped glasses and phonon sideband measurements are in progress. Figure 5 shows the result of a side-measurement performed on the cadmium mixed halide glass. The excitation spectra were measured by monitoring the $^5D_0$ - $^7F_0$ fluorescence as the sample was pumped by a rhodamine dye laser between 565 and 580 nm. The figure reveals an effective maximum phonon energy of 280 $cm^{-1}$ compared to the peaks of 240 $cm^{-1}$ and 370 $cm^{-1}$, corresponding to Cd-Cl and Cd-F obtained by Raman spectroscopy. The electron-phonon coupling constant is calculated using

$$g = \int I_{PSB}(\nu)d\nu \; / \int I_{PET}(\nu)d\nu \qquad (4)$$

where $I_{PSB}$ is the intensity of the phonon sideband and $I_{PET}$ is the intensity of the purely electronic transition, in this case centred at 580 nm. The ratio of the peak areas reveals a value of 0.26, compared to about 0.34 for fluorozironcate glass.

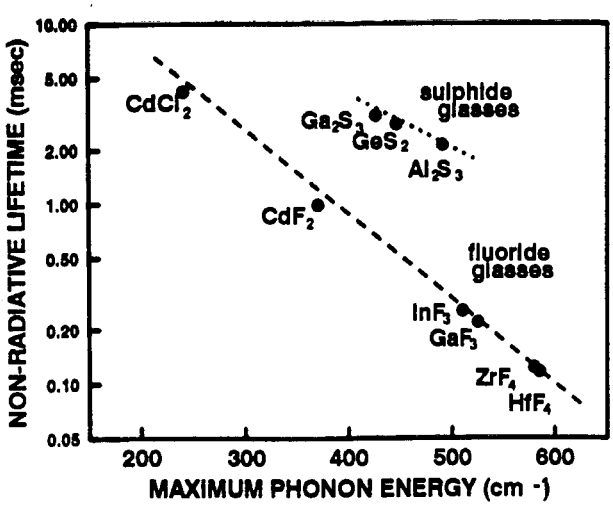


Figure 4. Non-radiative lifetimes for the $^1G_4$ level of $Pr^{3+}$-doped glasses as a function of the maximum phonon energy.

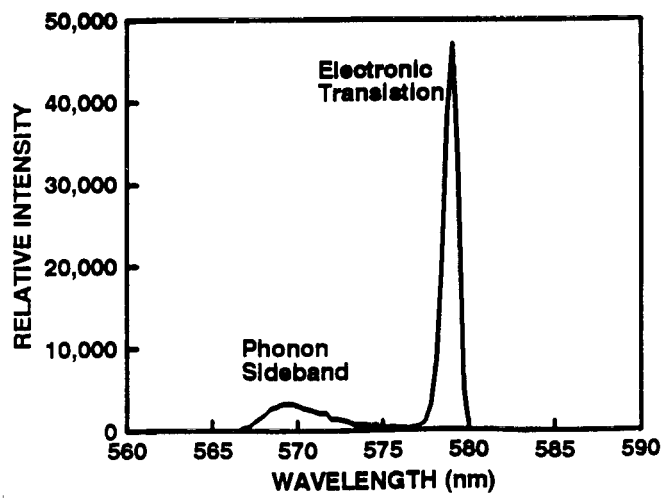


Figure 5. Phonon sideband measurement for $Eu^{3+}$-doped $CdF_2/CdCl_2$ glasses.

## 5. ABSORPTION SPECTROSCOPY

### 5.1 UV-VIS-NIR Spectroscopy

The absorption spectrum from the UV to near IR of undoped and heavily doped samples was measured at room temperature using a white light, dual beam, double grating spectrometer. Measurement range was 190-3200 nm with a resolution of 0.25 nm. A polished bulk glass sample was placed in one path, and the reference path was either empty, contained an identical sample of reduced thickness or an identical undoped sample of the same thickness. In the first of the above three cases, transmission was corrected for reflection from the sample endfaces.

Figure 6 shows the absorption spectrum of $Pr^{3+}$ in a fluoride ($HfF_4$) and sulphide ($Ga_2S_3$) glass. Among the halide glasses, little difference between the absorption bands is found. Peak positions are identical though there is variation in the peak areas, ie. the integrated absorption coefficient and thus the oscillator strengths, as calculated in the next section. Table 3 provides the absorption peak positions for these two families of glasses. Transmission measurements through a polished bulk sample provide the first indication of the suitability of a host for application in the visible and near infrared. Unfortunately, the trend to lower phonon energies parallels a shift in the ultraviolet cut-off towards the IR. For upconversion lasers and optical amplifiers operating in the second telecommunications window, this is of critical concern. In section 5.4 we combine this UV-VIS-NIR data with that obtained further into the infrared and determine the total useful transmission range of our glasses.

**Table 3. Energy level positions for fluoride based glasses and $Ga_2S_3$.**

| Energy Level | Wavelength (nm) | |
|---|---|---|
| | Fluoride | $Ga_2S_3$ |
| $^3P_2$ | 441 | 450 |
| $^3P_1 + {}^1I_6$ | 466 | 473 |
| $^3P_0$ | 478 | 491 |
| $^1D_2$ | 589 | 594 |
| $^1G_4$ | 1010 | 996 |
| $^3F_4$ | 1441 | 1402 |
| $^3F_3$ | 1541 | 1535 |
| $^3F_2$ | 1942 | 1896 |
| $^3H_6$ | 2253 | 2360 |

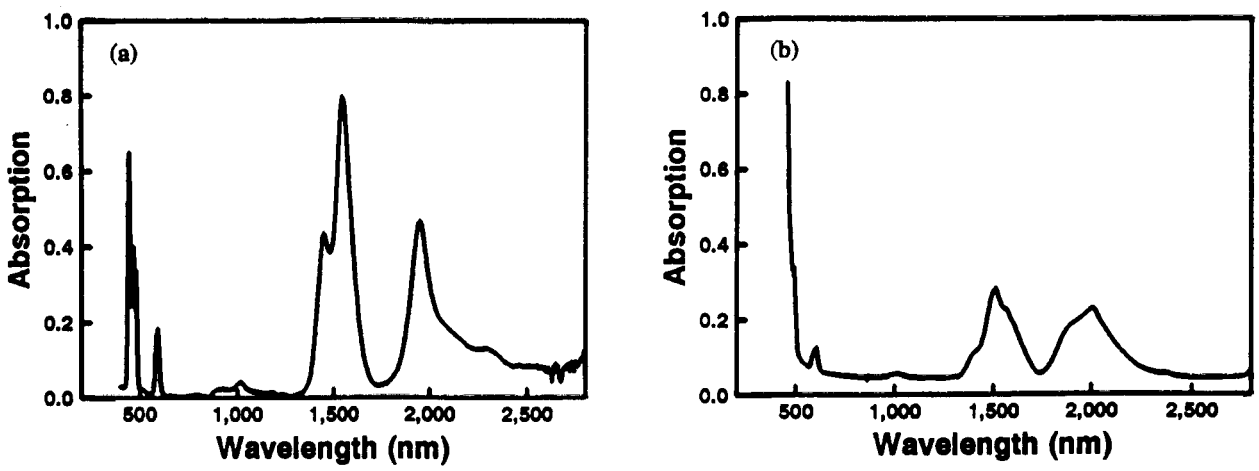


**Figure 6. Absorption bands of $Pr^{3+}$ in (a) $HfF_4$ and (b) $Ga_2S_3$based glass. Peak positions are are identified in table 3.**

### 5.2 Judd-Ofelt Theory

The transitions which occur between the ground state $4f^N$ configuration of the trivalent rare earth can be accounted for by a theory developed by both Judd[31] and Ofelt[32]. They have show that the possibilities for electric-dipole transitions can be expressed as sum of a small number of terms involving parameters which contain the strength of the configuration mixing. In the Judd-Ofelt (J-O) theory, the electric dipole oscillator strength of a transition of average frequency ν from a level J to a level J′ is given by

$$f(aJ;bJ') = \frac{8\pi^2 m\nu}{3h(2J+1)e^2 n(\lambda)^2} \frac{n(\lambda)[n(\lambda)^2+2)]^2}{9} S_{ed}(aJ,bJ') \tag{5}$$

where $n(\lambda)$ is the refractive index of the medium as a function of wavelength. The parameters m, e and h are the electronic mass, charge and Planks constant, respectively. In what we call standard J-O theory, the electric dipole line strength $S_{ed}$ is given by:

$$S_{ed} = e^2 \sum_{t=2,4,6} \Omega_t (\langle 4f^n | U^t | 4f^n J' \rangle)^2 \tag{6}$$

where $\Omega_t$ are the three phenomenological J-O parameters. The doubly reduced matrix elements of the tensor operator $U^{(t)}$, for $Pr^{3+}$ in $LaF_3$ have been calculated by Weber[33]. Their values are assumed to be independent of the host. The experimental oscillator strengths are found by measurement of the integrated absorption coefficient for each of the various transitions and using the expression:

$$f(aJ;bJ') = \frac{mc^2}{N\pi e^2} \int \frac{2.303\ OD(\lambda) d\lambda}{d\lambda^2} \tag{7}$$

Here c is the speed of light, N is the number of active ions per unit volume and $OD(\lambda)$ is the optical density. By fitting the experimental oscillator strengths given by equation (7) to the theoretical oscillator strength given by equations (5) and (6), the $\Omega_t$ parameters are derived. Table 4 presents the experimental oscillator strengths for our series of halide glasses, as calculated by equation (7). The corresponding J-O parameters are given in Table 5.

**Table 4. Measured oscillator strengths of $Pr^{+3}$ in $ZrF_4$, $HfF_4$, $GaF_3$, $InF_3$ and $CdF_3$ glasses. All transitions are from the $^3H_4$ fundamental level to the level indicated.**

| Transition | Experimental Oscillator Strength x $10^{-6}$ | | | | | |
|---|---|---|---|---|---|---|
| | ZBLAN | $HfF_4$ | $GaF_3$ | $InF_3$ | $CdF_2/Cl_2$ | $Ga_2S_3$ |
| $^3P_2$ | 1046 | 1218 | 1014 | 686 | 1463 | 1892 |
| $^3P_1 + {}^1I_6$ | 543 | 468 | 449 | 443 | 487 | 1405 |
| $^3P_0$ | 259 | 263 | 318 | 129 | 343 | 854 |
| $^1D_2$ | 225 | 224 | 234 | 150 | 212 | 395 |
| $^1G_4$ | 25 | 19 | 20 | 12 | 14 | 70 |
| $^3F_4$ | 249 | 285 | 204 | 138 | 311 | 280 |
| $^3F_3$ | 618 | 677 | 601 | 383 | 584 | 1356 |
| $^3F_2$ | 319 | 257 | 232 | 125 | 182 | 1144 |
| $^3H_6$ | 38 | 13 | 44 | 31 | 72 | 11 |

When applied to the 4f electrons of the $Pr^{+3}$ ion however, J-O theory often results in poor agreement between its theoretical predictions and experimental results[34-39]. This is seen both in the large deviation between the measured and calculated oscillator strengths and by the difficulty experienced in fitting the $^3H_4$ - $^3P_2$ and $^3H_4$ - $^1D_2$ hypersensitive transitions. In many of these cases, the J-O parameters which define the transition probabilities take on negative values, a case which has no physical meaning. Kornienko[39] has modified the Judd-Ofelt model to take into account the dependency of the J-O approximation on the higher energies of these manifolds. In this model, electron correlation effects are not considered and the electric-dipole line strength is given by:

$$S(aJ,bJ') = e^2 \sum_{t=2,4,6} \Omega'_t[1+2\alpha(E_{aJ}+E_{bJ'}-2E^0_f] \langle aJ\|U^t\|bJ'\rangle \qquad (8)$$

which replaces equation (6). Here $\Omega_t'$ are the modified J-O parameters and $\alpha$ is a parameter that for $Pr^{+3}$ has a value on the order of $10^{-5}$ $cm^{-1}$. Also introduced are $E_{aJ}$ and $E_{bJ'}$, the energies of aJ and bJ' levels respectively and $E^o_f$ which is the energy of the centre of gravity of the $4f^n$ configuration. For $Pr^{+3}$, this has a value of 9940 $cm^{-1}$. Comparison of the measured oscillator strengths for $CdF_2/CdCl_2$ glass with those calculated by the two methods is made in Table 6. Modified Judd-Ofelt parameters for the halide glasses are presented in Table 5. For sulphide based glasses, modified theory was not applied.

The results given in tables 5 and 6 show two advantages to the modified J-O treatment. First, Judd-Ofelt parameters are now all positive. This leads to the elimination of negative radiative rates and branching ratios. Second, there is an improvement in experimental fit between measured and calculated oscillator strengths, without the need for neglecting the hypersensitive $^3P_2$ level as is almost always the case for $Pr^{3+}$ doped glasses.

**Table 5. Standard and Modified Judd-Ofelt Parameters $\Omega_t$. For the standard theory, the $^3P_2$ oscillator strength not included.**

| Glass | Judd-Ofelt Parameters x $10^{-20}$ ($cm^2$) | | | | | | |
|---|---|---|---|---|---|---|---|
| | Standard Theory* | | | Modified Theory | | | |
| | $\Omega_2$ | $\Omega_4$ | $\Omega_6$ | $\Omega_2'$ | $\Omega_4'$ | $\Omega_6'$ | $\alpha$ x $10^{-5}$ |
| $ZrF_4$ | 2.0 | 4.5 | 5.3 | 14.1 | 3.5 | 15.6 | 0.25 |
| $HfF_4$ | 0.9 | 4.9 | 6.0 | 10.4 | 3.5 | 17.3 | 0.25 |
| $GaF_3$ | 0.3 | 5.0 | 4.8 | 9.0 | 3.9 | 13.8 | 0.25 |
| $InF_3$ | -0.1 | 3.6 | 2.9 | 7.4 | 3.1 | 9.3 | 0.25 |
| $CdF_2/Cl_2$ | -1.2 | 5.1 | 5.1 | 5.0 | 3.8 | 18.9 | 0.27 |
| $Ga_2S_3$ | 7.3 | 6.2 | 3.9 | | | | |

The optical properties of the glasses such as radiative rates, total radiative lifetimes and branching ratios for all transitions can be calculated directly from the J-O parameters. Herein lies the strength and usefulness of the Judd-Ofelt theory. From measurement of a few absorption bands, all the radiative properties of an ion in a host can be derived, generally to an uncertainty of ± 20%.

The spontaneous emission probability can be estimated using the $\Omega_t$ parameters and the expression:

$$A(aJ;bJ') = \frac{64\pi^4\nu^3}{3(2J+1)hc^3}\frac{n(n^2+2)^2}{9}S_{ed} \qquad (9)$$

Which is related to the radiative lifetime $\tau$ of excited state by:

$$\tau_a^{-1} = \sum_b (A_{aJ,bJ'}) \quad (10)$$

where $A_{aJ,bJ'}$ are the radiative transition probabilities from level a to level b, and the summation is over all terminal levels. Branching ratios for each level follow directly from the radiative lifetimes.

**Table 6. Measured and Calculated Oscillator Strengths determined by Judd-Ofelt Standard and Modified Theory.**

| Transition | Oscillator Strength (x $10^{-8}$) | | |
|---|---|---|---|
| | Experimental | Standard J-O | Modified J-O |
| $^3P_2$ | 1463 | 684 | 1369 |
| $^3P_1 + {}^1I_6$ | 487 | 488 | 555 |
| $^3P_0$ | 343 | 318 | 281 |
| $^1D_2$ | 212 | 178 | 330 |
| $^1G_4$ | 14 | 23 | 37 |
| $^3F_4$ | 311 | 622 | 528 |
| $^3F_3$ | 584 | 957 | 503 |
| $^3F_2$ | 182 | 107 | 155 |
| $^3H_6$ | 72 | 131 | 47 |
| rms x $10^{-8}$ | | 377 | 120 |

### 5.3 Infrared Spectroscopy and Intrinsic Loss

Infrared absorption and transmission measurements were performed on a commercial Fourier transform infrared spectrometer (FTIR). Resolution was 4.0 $cm^{-1}$ over the measurement range $6500^{-1}$ to 400 $cm^{-1}$ (1.5-25 μm). Figure 7 shows the results of a measurement performed on an undoped sample of $Ga_2S_3$ glass. Many impurities commonly found in halide and sulphide glasses have their fundamental absorptions in the wavelength range covered by these instruments[40]. Table 7 identifies some of the principal impurity absorptions. We note that oxide impurities in the form of $OH^-$ and $SO_4^{-2}$ dominate in this sulphide glass.

The total intrinsic optical attenuation can now be expressed in the familiar form[45]:

$$\alpha = A_1 \exp(A_2/\lambda) + B_1 \exp(B_2/\lambda) + (C/\lambda^4) \quad (11)$$

where $A_1$, $A_2$, $B_1$ , $B_2$ and C are constants. The first two terms are determined by fitting the experimental absorption spectra obtained in the visible and infrared to an exponential. The first term represents UV edge, the second the IR edge arising from multiphonon absorption. The third term represents Rayleigh scattering and is given by the characteristic $\lambda^{-4}$ wavelength dependence with the constant C given by

$$C = 8/3\pi^3(n^2-1)^2\beta kT_g \quad (12)$$

where n is the refractive index, β is the isothermal compressibility, k = 1.38 x $10^{-23}$ Nm/K is Boltzman's constant and $T_g$ is the glass transition temperature of the glass.

Determination of the absolute intrinsic loss minimum therefore requires knowledge of mechanical properties,

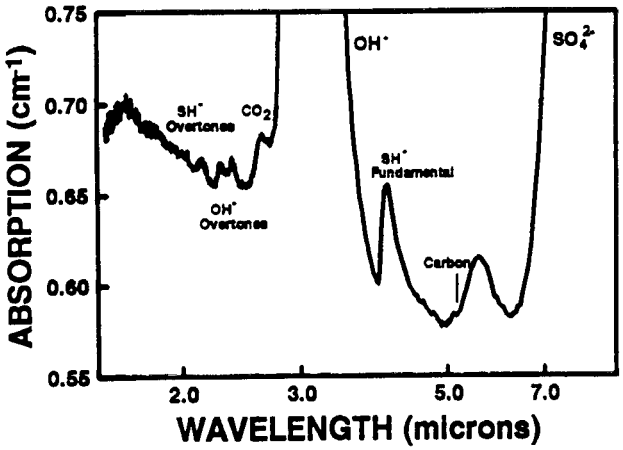


Figure 7. FTIR measurements of absorption in an $Ga_2S_3$ glass.

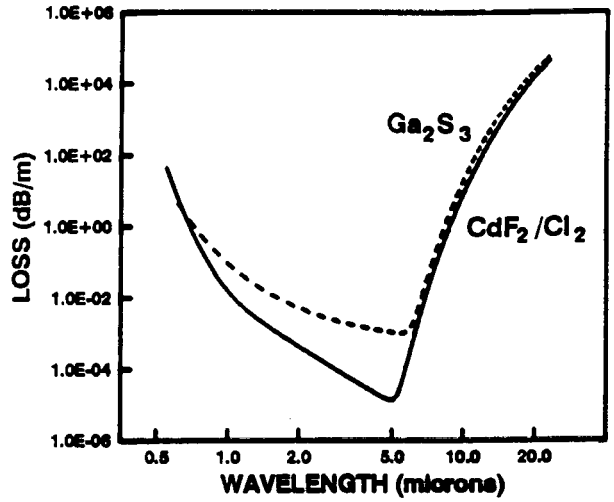


Figure 8. V-curve composite of three sources of intrinsic loss of $CdF_2/Cl_2$ and $Ga_2S_3$ glasses.

which are not often conveniently obtained. The compressibility of glasses is low however, and is not expected to vary significantly. Values for the Youngs modulus and bulk modulus of a series of halide glasses has been tabulated by Drexhage[19]. For the mixed cadmium halide, we approximate $\beta = 2.0 \times 10^{-3}$ kbar$^{-1}$, which is the value for $ZrF_4$-based glasses. For our sulphide glasses, we use the value for $GeS_2$ based glasses[41], $\beta = 8.54 \times 10^{-3}$ kbar$^{-1}$. In any case, as the V-curves to follow will show, even two orders of magnitude difference in this term will have a negligible effect on the position of the loss minimum and the total minimum loss at 1.3 microns. It would appear that a relatively high value for $T_g$ would be a disadvantage compared to other lower $T_g$ chalcogenide glasses. However, Nishii[42] shows that defect related mid-gap absorptions limit the transmission loss in chalcogenides and that a low glass transition temperature is a distinct disadvantage since this leads to high defect formation.

The total intrinsic loss, obtained using equation (11), is shown in figure 8, for the $CdF_2/Cl_2$ and $Ga_2S_3$ glasses. For chalcogenide glasses in general, there is some speculation, however, as to whether minimum loss for chalcogenides is determined by the Rayleigh scattering limit, or by a weak absorption tail extending from the UV edge[43]. In addition, in multicomponent glasses such as these, compositional variations may contribute more to Rayleigh scattering than equation (12) indicates[44].

## 6. FLUORESCENCE MEASUREMENT

### 6.1 Fluorescence Spectra

The fluorescence spectra were obtained by pumping with either a Ti:Sapphire laser tuned to the peak of the $^1G_4$ ground state absorption, a dye laser tuned to the $^1D_2$ level or by an argon ion laser pumping into the $^3P$ manifold, and then analyzing the emission on an optical spectrum analyzer. By chopping the signal with an acousto-optic modulator and directly detecting the decay of the fluorescence intensity, the lifetime of these levels could be determined. Figures 9-11 provide fluorescence spectra obtained from excitation at 1020, 514.5 and 497.6 nm, respectively.

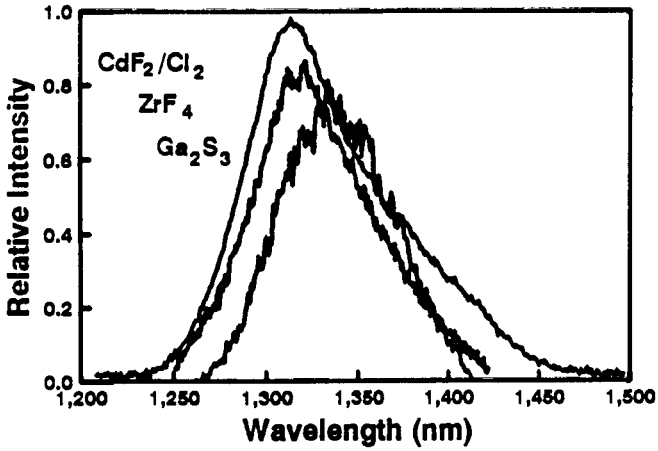


Figure 9. Fluorescence obtained by excitation of the $^1G_4$ level by 1020 nm pump.

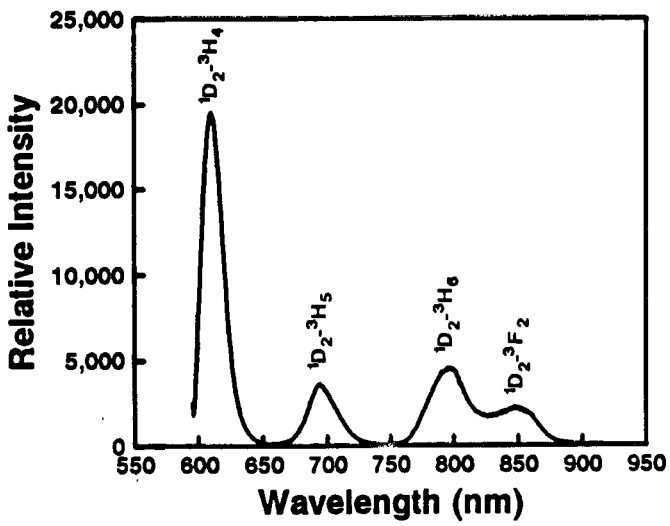


Figure 10. Fluorescence obtained by excitation of the $^1D_2$ level by 5145 nm pump in a fluoride glass.

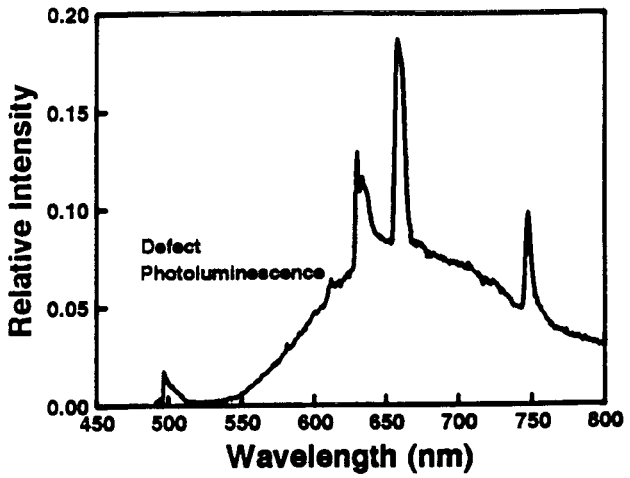


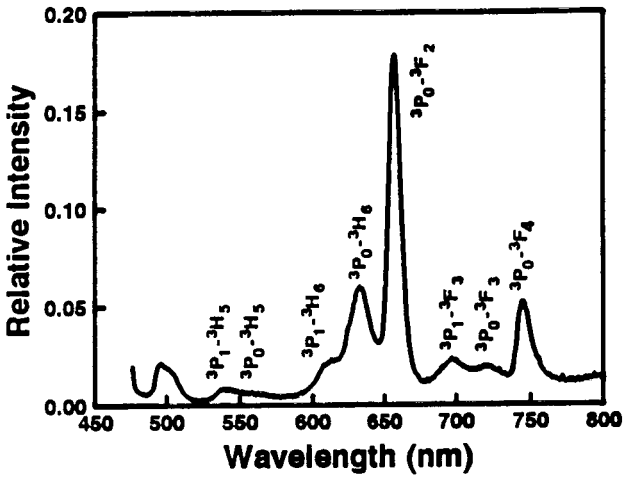


Figure 11. Photoluminescence and $^3P_0$ fluorescence observed at (a) 4K and (b) room temperature for $Ga_2S_3$ glass.

Figure 11(a) shows a low-temperature fluorescence measurement, obtained by pumping into the $^3P$ manifold while maintaining a sample temperature of 4 K through liquid helium cooling[45]. In contrast to the room temperature emission shown in figure 11(b), a broad visible luminescence is observed completely covering the visible spectrum. The origin of this luminescence is defects in the glass structure, attributed to sulphur loss, and caused by uncoordinated atoms or dangling bonds[46]. Implications of this defect structure are not clear but they may be detrimental in two ways. First, as acting as sites for non-radiative quenching of the excited rare-earth ion and second, contributing to a weak absorption which may contribute to the intrinsic loss.

### 6.2 Measured Lifetime

Table 8 summarizes the results of measurements of the decay time after excitation of the $^1G_4$ manifold. Pump wavelength was chosen to maximize the intensity of the 1.3 μm emission. The emission lifetime is defined as

$$\tau_m = \int I(t)dt / I(0) \qquad (13)$$

which, for a perfectly exponential decay, corresponds to the 1/e intensity decrement. For non-exponential decay, the measured lifetime $\tau_m$, defined by (13) provides an average of the different e-folding time.

In Table 9, we compare the measured $^1D_2$ lifetime with that obtained by both Judd-Ofelt standard and modified theory. For this level, the lifetime is completely dominated by radiative decay. It is clear from these results the superiority of modified Judd-Ofelt theory over the standard theory, in predicting the radiative lifetimes.

**Table 8. Measured $^1G_4$ Lifetimes for the series of glasses doped with less than 1000 ppm/wt $Pr^{3+}$.**

| Glass | Measured Lifetime (μsec) | 1/e Lifetime (μsec) |
|---|---|---|
| $ZrF_4$ | 167 | 129 |
| $HfF_4$ | 147 | 133 |
| $GaF_3$ | 261 | 188 |
| $InF_3$ | 381 | 208 |
| $CdF_2/Cl_2$ | 342 | 322 |
| $Ga_2S_3$ | 273 | 264 |

**Table 9. Measured $^1D_2$ lifetime compared to calculated lifetime obtained by standard and modified Judd-Ofelt theory. The $^3P_2$ oscillator strength was omitted in the standard calculation.**

| Glass | Lifetime (μsec) | | |
|---|---|---|---|
| | Measured | Standard | Modified |
| $ZrF_4$ | 387 | 510 | 241 |
| $HfF_4$ | 306 | 534 | 259 |
| $GaF_3$ | 217 | 603 | 288 |
| $InF_3$ | 400 | 1050 | 399 |
| $CdF_2/Cl_2$ | 335 | 781 | 285 |

## 7. TOTAL DECAY RATES

### 7.1 Quantum Efficiency

For an excited level of a rare earth ion in any glass, the observed fluorescence decay rate ($W_m$) is governed by the rate of radiative emission ($W_R$), the multiphonon decay rate ($W_{nr}$) and the rate of energy transfer to quenching centres ($W_{ET}$). We can write

$$W_m = W_R + W_{nr} + W_{ET} \quad \text{or} \quad \tau_m = 1/\tau_R + 1/\tau_{nr} + 1/\tau_{ET} \qquad (14)$$

where $\tau_m$ is the measured lifetime and $\tau_R$, $\tau_{nr}$ and $\tau_{ET}$ are the lifetimes corresponding to the radiative rates. In the absence of any impurities and quenching centres, and for ion concentrations sufficiently low so that ion-ion interaction is negligible, the measured lifetime should then follow directly from the sum of the radiative and non-radiative rates. Table 10 provides measured and calculated lifetimes for the $^3P_0$, $^1D_2$ and $^1G_4$ energy levels of our glasses of interest.

Quantum efficiency follows from the radiative and non-radiative rates. Defined as the ratio of pump

photons emitted radiatively to the total number of pump photons, this is calculated from the ratio of the radiative to total decay rate. Our theoretical quantum efficiencies are based on the calculated radiative and non-radiative rates, our experimental quantum efficiencies use the measured rate and the total calculated rate. Figure 12 plots the measured and calculated quantum efficiencies for the glasses studied.

**Table 10. Radiative and Non-Radiative Lifetimes for the $^3P_0$, $^1D_2$ and $^1G_4$ energy levels of $Pr^{3+}$-doped glasses ($^1D_2$ radiative rates calculated using the modified Judd-Ofelt treatment).**

| Glass | Energy Levels | Radiative Lifetime (μsec) | Non-Radiative Lifetime (μsec) | Total Lifetime (μsec) | Measured Lifetime (μsec) |
|---|---|---|---|---|---|
| $ZrF_4$ | $^1G_4$ | 2880 | 123 | 118 | 129 |
| | $^1D_2$ | 241 | - | 241 | 387 |
| | $^3P_0$ | 37 | 20080 | 37 | 48 |
| $HfF_4$ | $^1G_4$ | 2710 | 117 | 112 | 133 |
| | $^1D_2$ | 317 | - | 317 | 306 |
| | $^3P_0$ | 38 | 19070 | 38 | n/a |
| $GaF_3$ | $^1G_4$ | 3010 | 218 | 203 | 188 |
| | $^1D_2$ | 288 | - | 288 | 217 |
| | $^3P_0$ | 38 | 27300 | 38 | n/a |
| $InF_3$ | $^1G_4$ | 5000 | 254 | 230 | 208 |
| | $^1D_2$ | 399 | - | 399 | 400 |
| | $^3P_0$ | 59 | 41530 | 59 | 48 |
| $CdF_2/Cl_2$ | $^1G_4$ | 2870 | 980 | 730 | 322 |
| | $^1D_2$ | 285 | - | 285 | 335 |
| | $^3P_0$ | 40 | - | 40 | 35 |
| $Ga_2S_3$ | $^1G_4$ | 510 | 2010 | 407 | 264 |
| | $^1D_2$ | 56 | - | 56 | 57 |
| | $^3P_0$ | 5 | 18960 | 5 | 4 |

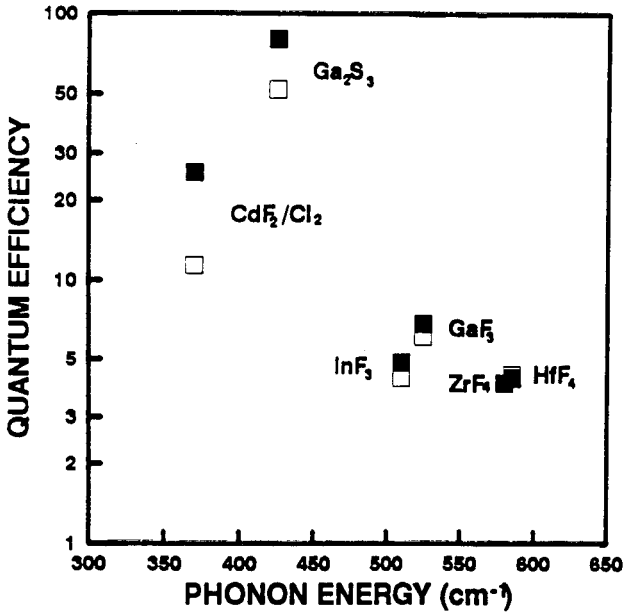


Figure 12. Calculated and measured quantum efficiencies as a function of the maximum phonon energy for each glass host.

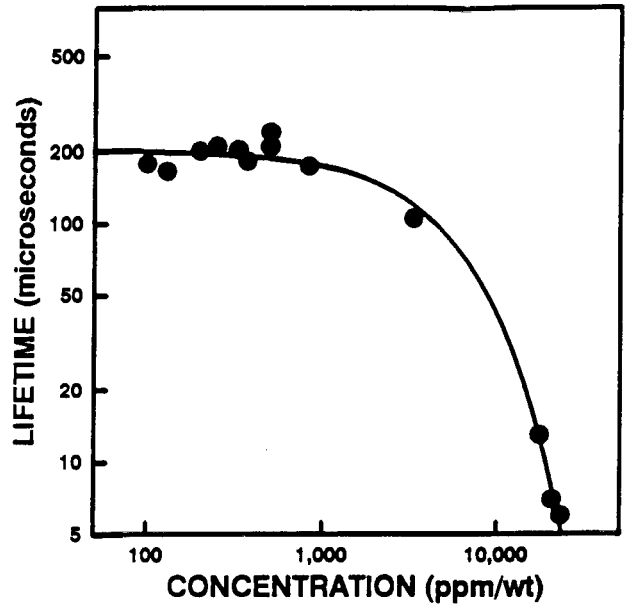


Figure 13. Measured lifetime as a function of $Pr^{3+}$ concentration, showing quenching in $Ga_2S_3$ glass.

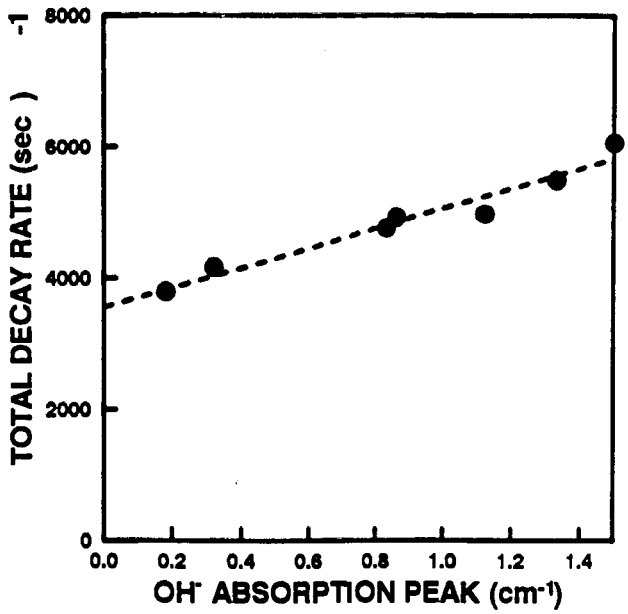


Figure 14. The influence of OH content on the measured lifetime for $Ga_2S_3$ glass.

### 7.2 Quenching

As the $Pr^{3+}$ concentration increases beyond about 1000 ppm wt, quenching of the fluorescence through ion-ion interaction sets in. This undesirable energy transfer mechanism sets an upper limit to the maximum ion concentration in the glass. Figure 13 plots the measured lifetime as a function of $Pr^{3+}$ concentration for a $Ga_2S_3$ glass. A similar dependence was obtained by Ohishi[3] for $Pr^{3+}$-doped ZBLAN. These results indicate that independent of the host, ion-ion interacts limit the maximum concentrations to under 1000 ppm of $Pr^{3+}$. For the $^1G_4$ transition, this necessitates fibre lengths of a minimum of about 10 $m^{1-3}$, in order to achieve sufficient pump absorption.

Figure 14 shows the influence of $OH^-$ content on the measured lifetime for $Ga_2S_3$ glass. Impurities, as identified by FTIR, are known to act as quenching centres for an excited ion. In particular, through FTIR measurements, we have quantified the relationship between $OH^-$ peak height at 3.0 microns and the measured lifetime. Clearly, $OH^-$ plays a role in quenching, probably through the $OH^-$ combination band centred at 1.38 microns. Extrapolating the line to the intercept yields the expected total rate for complete elimination of $OH^-$, in this case, 3546 $sec^{-1}$ or 282 μsec.

## 8. SUMMARY

In summary, we have fabricated and spectroscopically evaluated a series of halide and sulphide glasses doped with $Pr^{3+}$. This paper reviews the procedure we have used to assess the suitability of these low-phonon-energy glasses to applications at 1.3 microns. The procedure and results though, are applicable to the study of all transitions and thus other applications of these or related glasses.

## 9. ACKNOWLEDGEMENTS

This work was supported by a UK SERC/DTI LINK programme (GOAL) and an EC RACE project (FLUOR/II). Chalcogenide materials were supplied by Merck Ltd., Poole, Dorset, UK.

## 10. REFERENCES

1. Y. Durteste, M. Monerie, J.Y. Allain and H. Poigant, "Amplification and Lasing at 1.3 μm in Praseodynium-Doped Fluorozirconate Fibres", *Electron. Lett.*, Vol. 27, pp. 626-628, April 1991.
2. S.F. Carter, D. Szebesta, S.T. Davey, R. Wyatt, M.C. Brierley and P.W. France, "Amplification at 1.3 μm in a $Pr^{3+}$-doped Single-Mode Fluorozirconate Fibre", *Electron. Lett.*, Vol. 27, pp. 628-629, April 1991.
3. Y. Ohishi, T. Kanamori and S. Takashasi, "Concentration Quenching in $Pr^{3+}$-doped Fluoride Fibre Amplifier Operating at 1.3 μm", Proceeding 17th European Conference on Optical Communication, Paper MoA2, Paris, 1991.
4. S.T. Davey, D. Szebesta, J.R. Williams, T. Whitley, R. Wyatt, "Rare Earth Doped, High NA Fluoride Fibre Amplifiers", Proc. *8th Int. Symposium on Halide Glass*, Perros-Guirec, France, pp. 458-462, Sept. 1992.
5. Y. Ohishi, T. Kanamori, T. Nishi, Y. Nishida and S. Takahashi, "Quantum efficiency at 1.3 μm of $Pr^{3+}$ in infrared glasses", *Proc. 16th Int. Congress on Glass*, pp. 73-78, Madrid, Sept. 1992.
6. P.C. Becker, M.M. Broer, V.G. Lambrecht, A.J. Bruce and G. Nykolak, "$Pr^{3+}$: La-Ga-S glass: A promising material for 1.3 μm fibre amplification", *Proc. OAA'92*, Postdeadline paper PD5, pp. 20-23, Santa Fe, 1992.
7. M.A. Newhouse, R.F. Bartholomew, B.G. Aitken, A.L. Saad and N.F. Borrelli, "309 μsec $Pr^{3+}$ excited state lifetime observed in a mixed halide glass", pp. 70-73, *Proc. OAA'92*, Postdeadline paper PD 16, Santa Fe, 1992.
8. R.S. Deol, D.W. Hewak, S. Jordery, A. Jha, M. Poulain, M.D. Baro, D.N. Payne, "Improved fluoride glasses for 1.3 μm optical amplifiers", Proc. *8th Int. Symposium on Halide Glass*, Perros-Guirec, France, pp. 443-447, Sept. 1992.
9. D.W. Hewak, R.S. Deol, J. Wang, G. Wylangowski, J.A. Medeiros, B. Samson, R.I. Laming, W.S. Brocklesby, D.N. Payne, A. Jha, M. Poulain, S. Otero, S. Surinach, and M.D. Baro, "Low phonon-energy glasses for efficient 1.3 μm optical fibre amplifiers', *Electron. Lett.*, Vol. 29, pp. 237-238, Jan. 1993.
10. M. Shimizu, M. Yamada, M. Monguchi, T. Takeshita and M. Okayasu, "Erbium-doped fibre amplifiers with an extremely high gain coefficient of 11.0 dB/mW", *Electron. Lett.*, Vol. 26, pp. 1641-1642, 1990.
11. C.M. Baldwin and J.D. Mackenzie, "Fundamental Conditions for Glass Formation in Fluoride Systems", *J. Am. Ceram. Soc.*, Vol. 62, pp. 537-538, 1979.
12. M. Poulain, M. Poulain, Y. Messaddeq and A. Soufiane, "Fluoroindate Glasses", to be published by the American Ceramic Society in *Solid State Optical Materials*, 1992.

13. A. Jha and J.M. Parker, "Preparation of infrared transmiting $CdF_2$ based mixed halide glasses", *Physics and Chemistry of Glasses*, Vol. 32, pp. 1-12, Feb. 1991.
14. M. Matecki and M. Poulain, "Composition adjustments in cadmium fluorochloride glasses", *J. Non. Crystalline Solids*, Vol. 140, p. 82-86, 1992.
15. P.N. Kumta and S. H. Risbud, "Novel Glasses in Rare-Earth Sulfides", *Ceramic Bulletin*, Vol. 69, pp. 1977-1984, 1977.
16. J. Flahaut, M. Guittard and A.M. Loireau-Lozac'h, "Rare earth sulphide and oxysulphide glasses", *Glass Technology*, Vol. 24, pp. 149-156, 1983.
17. E. Comyns, editor, *Fluoride Glasses*, Society of Chemical Industry, 1989.
18. T. Katsuyama and H. Matsumura, *Infrared Optical Fibers*, Adam Higler Series on Optics and Optoelectronics, Bristol, England, 1989.
19. M.G. Drexhage, "Heavy-Metal Fluoride Glasses", *Treatise on Materials Science and Technology*, ed., M. Tomozawa and R.H. Doremus, Vol. 26, pp. 141-243, 1985.
20. M. Poulain, "Fluoride Glass Composition and Processing", *Fluoride Glass Fibre Optics*, eds. I.D. Aggarwal and G. Lu, Chapter 2., Academic House, San Diego, 1991.
21. A.M. Lozac'h, S. Barnier, M. Guittard, P. Besancon and J. Flahaut, "Propietes optiques des verres de chalcogenures de terre rares", *Ann. Chim.*, Vol. 9, pp. 127-132, 1974.
22. I.W. Donald and P.W. McMillan, "Review: Infrared Transmitting Materials", *J. Mater. Sci.*, Vol. 13, pp. 1151-1176, 1978.
23. B. Bendow, P.K. Banerjee and M.G. Drexhage, "Comparative study of Vibrational Characteristics of Fluorozirconate and Fluorohafnate Glasses", *Communications of the American Ceramic Society*, pp. C8-C9, January 1982.
24. J.R. Lincoln, *Spectroscopy of Rare Earth Doped Glasses*, PhD. Thesis, Department of Physics, University of Southampton, Nov. 1992.
25. R. Reisfeld and C.K. Jorgensen, "Excited state phenomena in vitreous materials', Handbook on the Physics and Chemistry of Rare Earths, Chapter 58, Elsevier Science Publishers B.V., 1987.
26. D.R. Tallant and B. Bendow, *Raman study of Composition Dependence and Crystallization Phenomena in Heavy Metal Fluoride Glasses*, Materials Science Forum, Vol. 6, pp. 533-542, 1985.
27. R.W. Wood, *Physical Optics*, MacMillan, New York, 1934.
28. C.B. Layne, W.H. Lowdermilk and M.J. Weber, "Multiphonon relaxation of rare-earth ions in oxide glasses', *Phys. Rev. B.*, Vol. 16, pp. 10-20, 1977.
29. R. Engleman, *Nonradiative decay of Ions and Molecules*, North Holland, Amsterdam, New York, Oxford, 1979.
30. K. Soga, H. Inoue and A. Makishima, "Fluorescence properties of fluorozirconate glasses containing $Eu^{3+}$ ions", *Journal of Luminescence*, Vol. 55 pp. 17-25, 1993.
31. B.R. Judd, "Optical Absorption Intensities of Rare-Earth Ions", *Phys. Rev.*, Vol. 127, pp. 750-761, 1962.
32. G.S. Ofelt, "Intensities of Crystal Spectra of Rare-Earth Ions", *J.Chem.Phys.*, Vol. 37, pp. 511- 520, 1962.
33. M.J. Weber, "Spontaneous emission probabilities and quantum efficiencies for excited states of $Pr^{3+}$ in $LaF_3$", *J. Chem. Phys.*, Vol. 48, pp. 4774-4780, 1968.
34. J. Hormadaly and R. Reisfeld, "Intensity Parameters and Laser Analysis of $Pr^{3+}$ and $Dy^{3+}$ in Oxide Glasses", *J. Non-Crystalline Solids*, Vol. 30, pp. 337-348, 1979.
35. M. Eyal, E. Greenberg, R. Reisfeld and N. Spector, "Spectroscopy of Praseodynium(III) in Zirconium Fluoride Glass", *Chemical Physics Letters*, Vol. 117, pp. 108-114 1985.
36. J.L.Adam and W.A.Sibley, "Optical Transitions of $Pr^{3+}$ Ions in Fluorozirconate Glass", *J. Non-Crystalline Solids*, Vol. 76, pp. 267-279, 1985.
37. G.Amaranath, S.Buddhudu, F.J. Bryant, Luo Xi, B. Yu and S. Huang, "Spectroscopic properties of $Pr^{3+}$-doped Multicomponent Fluoride Glasses", *Mat. Res. Bull.*, Vol. 25, pp. 1317-1323, 1990.
39. Kornienko, A.A., Kaminskii, A.A. and Dunina, E.B., "Dependence of the Line Strength of f-f Transitions on the Manifold Energy", *Phys. Status Solidi*, Vol. 157, pp. 267-273, 1990.
40. Poulain, M. and Saad, M.,"Absorption loss due to complex anions in Fluorozirconate Glasses", *J. Lightwave Tech.* Vol. LT-2, pp. 599-602, 1984.
41. S. Shibata, M. Horiguchi, K. Jinguji, S. Mitachi, T. Kanamori, T. Manabe, "Prediction of Loss Minima in Infrared Optical Fibres", *Electron. Lett.*, Vol. 17, pp.775-777, 1981.
42. J. Nishi, T. Yamashita and T. Yamagihi, "Low-loss chalcogenide glass fibre with core-cladding structure", *Appl. Phys. Lett.* Vol. 53, pp. 553-554, 1988.
43. T. Kanamori, Y. Terunuma, S. Takahashi and T. Miyashita, "Chalcogenide Glass Fibres for Mid-Infrared Transmission", *J. Lightwave. Tech.*, Vol. 2, pp. 607-613, Sept. 1984.
44. D.A. Pinnow, et al, *Appl. Phys. Lett.* Vol. 22, pp. 527-529. 1973.
45. W.S. Brocklesby and A.D. Pearson, "A spectroscopic study of Praseodynium-doped Gallium-Lanthanum-Sulphide Glass", submitted to the *J. of Luminescence*.
46. S.R. Elliot, 'Chalcogenide glasses', Material Science and Technology, Volume 9, *Glasses and Amorphous Materials*, Chapter 7 (Weinheim, New York)